nature structural & molecular biology

Repriming of DNA synthesis at stalled replication forks by human PrimPol

Silvana Mourón[1], Sara Rodriguez-Acebes[1,3], María I Martínez-Jiménez[2,3], Sara García-Gómez[2], Sandra Chocrón[2], Luis Blanco[2] & Juan Méndez[1]

DNA replication forks that collapse during the process of genomic duplication lead to double-strand breaks and constitute a threat to genomic stability. The risk of fork collapse is higher in the presence of replication inhibitors or after UV irradiation, which introduces specific modifications in the structure of DNA. In these cases, fork progression may be facilitated by error-prone translesion synthesis (TLS) DNA polymerases. Alternatively, the replisome may skip the damaged DNA, leaving an unreplicated gap to be repaired after replication. This mechanism strictly requires a priming event downstream of the lesion. Here we show that PrimPol, a new human primase and TLS polymerase, uses its primase activity to mediate uninterrupted fork progression after UV irradiation and to reinitiate DNA synthesis after dNTP depletion. As an enzyme involved in tolerance to DNA damage, PrimPol might become a target for cancer therapy.

During the process of genomic duplication, specialized enzymes called primases synthesize short RNA oligonucleotides that serve as 'primers' for DNA polymerases. The only human primase characterized to date (Polα-primase) initiates synthesis of the leading strand at each origin and synthesis of each Okazaki fragment in the lagging strand. RNA oligonucleotides made by primase are extended with dNTPs by Polα until a length of about 30 nucleotides and then passed on to polymerases Polδ and Polε[1]. The bulk of DNA synthesis is carried out by these processive polymerases, which are part of large 'replisome' structures that include the Cdc45-GINS-MCM (CMG) DNA helicase and multiple accessory proteins[2–4]. Despite their biochemical complexity, eukaryotic forks move at remarkable speeds, 1.5 kb/min on average[5]. Fork progression can be challenged by natural elements (for example, unusual DNA structures caused by sequence repeats or collision with the transcriptional machinery) or by lesions in the template DNA, such as base modifications, interstrand crosslinks or intrastrand adducts. In these situations, several responses have evolved to stabilize the replisome machinery, preventing its irreversible collapse that frequently results in double-strand breaks[6–8].

Lesions in the template DNA can be tolerated *in situ* by a group of polymerases adapted to perform TLS, such as Polη, Polι, Polκ, Polζ and Rev1 (refs. 9,10). The active site of these polymerases may use damaged DNA templates at the cost of being less selective in their incorporation of dNTPs into the nascent strand. Alternatively, lesions can be bypassed by the initiation of a new DNA strand downstream of the damaged area, leaving behind an unreplicated gap to be repaired post-replicatively. Evidence for such a 'lesion-skipping' mechanism, including the visualization of single-stranded DNA (ssDNA) gaps by electron microscopy[11] has been reported in bacteria, yeast and mammalian cells, particularly after UV irradiation[12–17]. This mechanism strictly requires a primase activity, to reinitiate DNA synthesis ahead of the lesion. The identity of the protein responsible for this activity remains unknown.

The product of *CCDC111* (*PRIMPOL*) gene, which contains the conserved motifs characteristic of the Archaeo-Eukaryotic primases (AEP) family[18], has been recently characterized as a second primase in human cells, the first capable of using dNTPs to make primers[19]. PrimPol is not only a DNA primase but also a TLS DNA polymerase as it tolerates templates with abasic sites or 8-oxoguanine modifications. Because a fraction of endogenous PrimPol is localized in the nucleus and the mitochondrial network, it has been postulated that it would have a role in tolerance of damage in both cellular compartments. Indeed, PrimPol gene silencing or ablation affects mitochondrial DNA replication[19]. In this work we investigated the possible function(s) of PrimPol during nuclear DNA replication. We report that its primase activity is a key element in promoting reinitiation of DNA synthesis when fork progression is challenged by UV irradiation or nucleotide attrition.

RESULTS

UV irradiation enhances PrimPol binding to chromatin

PrimPol mRNA expression peaks at G1–S phase, but the protein levels remain constant throughout the cell cycle (**Supplementary Fig. 1a**). Biochemical fractionation assays in synchronized cell cultures revealed that a fraction of PrimPol associated with nuclear chromatin mainly during the G1 and S phases of unperturbed cell cycles (**Fig. 1a**). The amount of PrimPol on chromatin increased upon

[1]Molecular Oncology Program, Spanish National Cancer Research Centre, Madrid, Spain. [2]Department of Genome Dynamics and Function, Centro de Biología Molecular "Severo Ochoa", Madrid, Spain. [3]These authors contributed equally to this work. Correspondence should be addressed to J.M. (jmendez@cnio.es) or L.B. (lblanco@cbm.uam.es).

Received 30 August; accepted 22 October; published online 17 November 2013; doi:10.1038/nsmb.2719

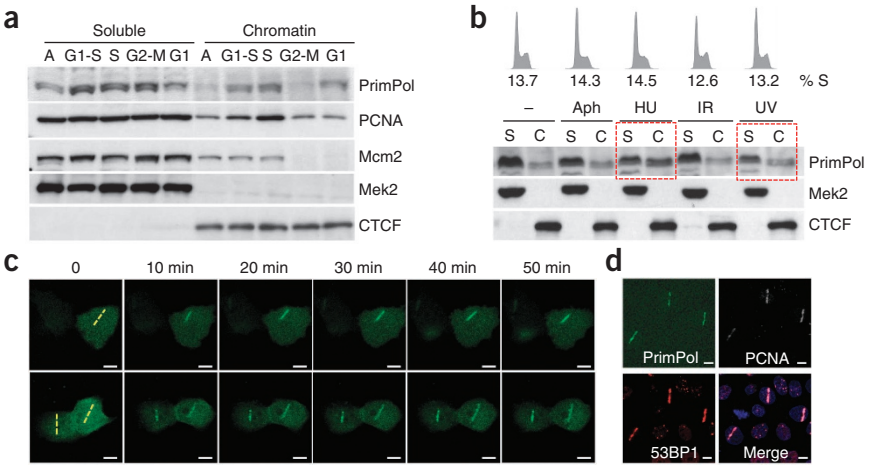

Figure 1 PrimPol associates with nuclear chromatin in unperturbed S phase and in response to DNA damage. (**a**) Distribution of PrimPol, PCNA and Mcm2 proteins between soluble and chromatin-bound fractions in cells synchronized at indicated stages of the cell cycle. A, asynchronous culture. Cytosolic Mek2 kinase and chromatin-bound CTCF are shown as controls for the biochemical fractionation. (**b**) Distribution of PrimPol between soluble (S) and chromatin (C) fractions in response to irradiation or exposure to replication inhibitors. Aph, 2 h in 10 μM aphidicolin; HU, 2 h in 2 mM hydroxyurea; IR, 10 Gy γ-irradiation; UV, 30 J/m2 irradiation. Mek2 and CTCF are shown as fractionation controls. Plots at the top show DNA-content profiles and percentage of cells in S phase after each treatment, as determined by flow cytometry after DNA staining with propidium iodide. Uncropped gel images are shown in **Supplementary Figure 7**. (**c**) Recruitment of GFP-PrimPol to sites of laser-induced DNA damage in HeLa cell nuclei (depicted as dashed yellow lines in the leftmost images). Time between laser irradiation and image acquisition is indicated. (**d**) Immunofluorescence detection of PrimPol, PCNA and 53BP1 in HeLa cells fixed 1 h after laser irradiation. Scale bars, 7.5 μm. Data are representative of three experiments (**a**,**b**), 38 laser-responsive cells, from a total of 106 irradiated cells (**c**) and 17 cells (**d**).

cellular exposure to replication inhibitor HU or UV irradiation (**Fig. 1b** and **Supplementary Fig. 1b**). We detected recruitment of PrimPol to chromatin in the presence of caffeine (an inhibitor of ATR and ATM kinases) or UCN-01 (an inhibitor of Chk1 kinase), suggesting that it occurs independently of the ATR-Chk1 checkpoint (**Supplementary Fig. 1c**). To investigate whether PrimPol is specifically recruited to sites of DNA damage, we transiently expressed a GFP-tagged PrimPol in HeLa or U20S cells and irradiated individual nuclei with an UV-A laser beam to locally induce DNA lesions. PrimPol was rapidly recruited to the laser path in both cell lines (**Fig. 1c** and **Supplementary Fig. 1d**) and colocalized with other proteins known to associate with damaged DNA such as PCNA and 53BP1 (**Fig. 1d**). These data suggest that PrimPol directly participates in the cellular response to DNA damage during chromosomal replication.

Replication stress and genomic instability upon PrimPol loss

To investigate PrimPol function, we generated stable cell lines carrying an inducible shRNA targeting the 3′ UTR of *PRIMPOL* gene (HeLa-, U2OS- and HDF-shPrimPol cells). In the presence of doxycycline, PrimPol was efficiently downregulated (**Fig. 2a**), and cells proliferated at a slightly slower pace without accumulating at any specific cell cycle stage (**Fig. 2b** and **Supplementary Fig. 2a**,**b**). Global incorporation of bromodeoxyuridine (BrdU) into nascent DNA was not affected (**Supplementary Fig. 2c**), but the percentage of cells displaying RPA foci almost doubled (**Fig. 2c**). Persistent RPA foci are normally indicative of replication stress, and we confirmed their presence in mouse embryonic fibroblasts (MEFs) derived from *Ccdc111*$^{-/-}$ (*Primpol*$^{-/-}$) embryos[19] (**Fig. 2d**). Another indication of replication stress was the higher intensity of γH2AX staining we observed by high-throughput confocal microscopy upon downregulation of PrimPol (**Fig. 2e**). After several division cycles in the absence of PrimPol, genetic instability was evidenced by the frequency of mitotic figures with misaligned and lagging chromosomes (**Supplementary Fig. 2d**) and the high percentage of interphase cells displaying micronuclei (**Fig. 2f**). Again, we observed these phenotypes in *Primpol*$^{-/-}$ MEFs (**Fig. 2f** and **Supplementary Fig. 2e**). In addition, primary T lymphocytes isolated from *Primpol*$^{-/-}$ mice and stimulated to proliferate *ex vivo* in the presence of aphidicolin showed a higher index of chromosomal breaks, gaps and fusions (**Fig. 2g** and **Supplementary Fig. 2f**,**g**). Therefore, genomic stability is compromised upon depletion of PrimPol in cultured cells.

PrimPol assists fork progression in an unperturbed S phase

Because PrimPol associated with chromatin in S phase and its downregulation caused replicative stress, we next analyzed the dynamics of DNA replication in HeLa-shPrimPol cells using stretched fibers[20]. We sequentially labeled cells growing in culture with two halogenated nucleotide analogs, chlorodeoxyuridine (CldU) and iododeoxyuridine (IdU), which we later detected by immunofluorescence. In the DNA fibers, moving forks are detected as bicolor tracks (magenta for CldU and green for IdU), and track length is proportional to the fork progression rate (FR; **Fig. 3a**). In addition, replication origins can be located as tricolor (green-magenta-green) tracks or at the intermediate point between two closely positioned forks moving away from each other[20]. First, we observed that FR was slower after PrimPol downregulation (median value of 0.47 kb/min, compared to 0.76 kb/min in control conditions; **Fig. 3a**,**b**). We confirmed the specificity of this effect by reintroduction of a plasmid encoding exogenous V5-tagged PrimPol, which resulted in normal FR values. In contrast, reintroduction of a PrimPol in which the two catalytic carboxylate residues Asp114 and Glu116 have been changed to alanines ('AxA' variant[19]), rendering the protein inactive, failed to recover normal FR values despite similar levels of protein expression (**Fig. 3b** and **Supplementary Fig. 3a**). Lower FR, also observed in *Primpol*$^{-/-}$ MEFs (**Fig. 3c**), could be explained by a higher frequency of fork stalling or a delay in the 'clearance' of stalled forks. In these assays we noticed that single-color first-label (magenta) tracks, which can only be generated by arrested forks or termination events, were more abundant in the absence of PrimPol (**Fig. 3d**). We also predicted that a higher frequency of stalled forks should induce the compensatory activation of 'dormant' origins[21–23]. Indeed, the average inter-origin distance (IOD) was significantly reduced upon downregulation of PrimPol (median of 60 kb, compared to 105 kb in control) or genetic ablation in MEFs (median of 84 kb in *Primpol*$^{-/-}$ cells, compared to 135 kb in control; **Fig. 3e**). Together, these results show that PrimPol operates during the S phase, facilitating fork progression even in the absence of exogenous sources of DNA damage.

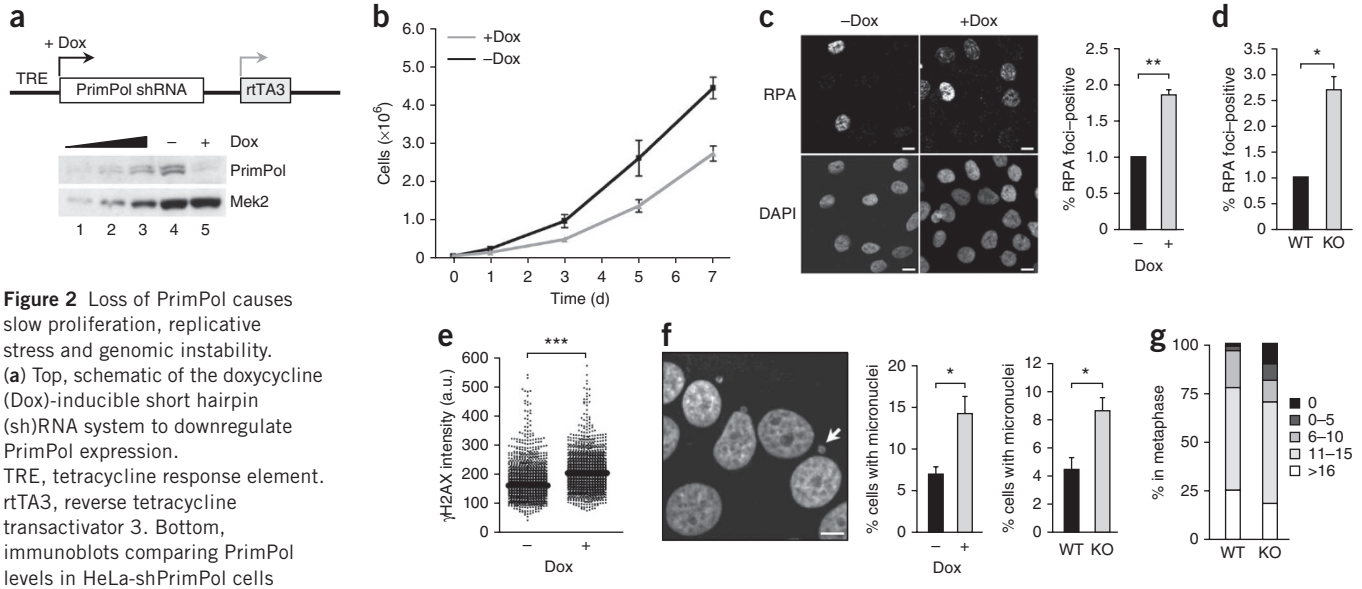

Figure 2 Loss of PrimPol causes slow proliferation, replicative stress and genomic instability. (**a**) Top, schematic of the doxycycline (Dox)-inducible short hairpin (sh)RNA system to downregulate PrimPol expression. TRE, tetracycline response element. rtTA3, reverse tetracycline transactivator 3. Bottom, immunoblots comparing PrimPol levels in HeLa-shPrimPol cells incubated with or without Dox for 72 h (lanes 4 and 5). Lanes 1–3 are serial dilutions (12.5%, 25% and 50%, respectively) of the sample analyzed in lane 4. Uncropped gel images are shown in **Supplementary Figure 7**. (**b**) Proliferation curves of HeLa-shPrimPol cells with (+) or without (–) Dox. (**c**) Left, micrographs showing RPA immunostaining in HeLa-shPrimPol cells with or without Dox. DNA was counterstained with DAPI. Scale bars, 10 μm. Right, percentages of RPA foci–positive cells. (**d**) Fold change of RPA foci–positive wild-type (WT) versus *Primpol*$^{-/-}$ (KO) MEFs. (**e**) γH2AX signal intensity, quantified by high-throughput microscopy, in HeLa-shPrimPol with or without Dox. Horizontal lines represent median values. (**f**) Images of micronuclei (white arrow) visualized by DAPI DNA staining in HeLa-shPrimPol cells. Scale bar, 5 μm. Histograms show the percentage of micronuclei-containing HeLa-shPrimPol cells with or without Dox (left), or WT versus *Primpol*$^{-/-}$ MEFs (right). (**g**) Chromosomal breaks and gaps detected in T lymphocytes obtained from WT or *Primpol*$^{-/-}$ (KO) mice after 2 d of concanavalin A (ConA)-induced proliferation. 0.4 μM aphidicolin was added to the medium for the last 24 h. Data are representative of ten experiments (**a**), pooled from seven experiments (**b**), pooled from three experiments (**c**–**e**), pooled from four experiments with HeLa-shPrimPol cells and three experiments with WT or *Primpol* $^{-/-}$ MEFs (**f**), and pooled from two mice of each genotype (**g**). Error bars, s.d. (**b**–**d**,**f**). $^{*}P < 0.05$ and $^{**}P < 0.01$ (Student's *t*-test; **c**,**d**,**f**), and $^{***}P < 0.001$ (**e**; Mann-Whitney test).

PrimPol mediates fork restart at UV light–induced lesions

We devised a variation of the DNA fiber assay to monitor the ability of replication forks to progress through specific challenges. We pulse-labeled HeLa-shPrimPol cells with CldU (magenta) and then irradiated them with UV light (30 J/m^2) before pulse-labeling them with IdU (green). In this setting, forks arrested by UV irradiation have incorporated only the first analog, whereas those that continued DNA synthesis should be labeled with both analogs (**Fig. 4a**). Loss of PrimPol markedly reduced the percentage of forks displaying continuous synthesis (**Fig. 4b**). This phenotype was fully reversed by cotransfection of a plasmid encoding wild-type PrimPol, but not the AxA catalytic variant (**Fig. 4b**). We observed similar effects when fork

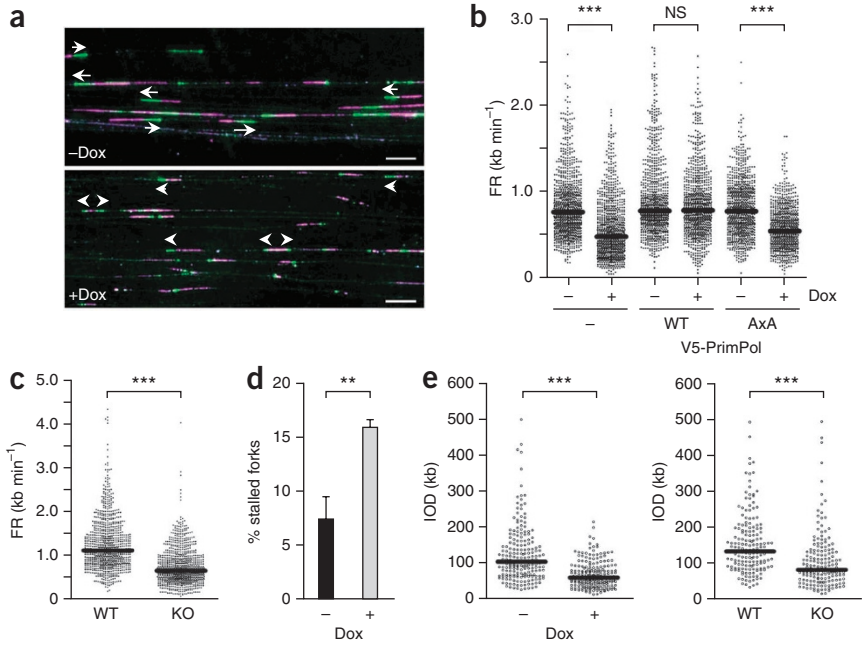

Figure 3 Slow fork progression after PrimPol downregulation. (**a**) Examples of DNA fibers labeled sequentially with CldU (magenta) and IdU (green), used to estimate FR and IOD in HeLa-shPrimPol cells without Dox or treated with Dox. Scale bars, 10 μm. (**b**) FR values calculated from stretched fibers, as those shown in **a**. Where indicated, plasmids encoding V5-tagged wild-type (WT) or AxA PrimPol proteins were cotransfected into HeLa-shPrimPol cells. (**c**) FR values in MEFs derived from WT and *Primpol*$^{-/-}$ (KO) mice. (**d**) Percentage of single-color magenta tracks relative to bicolor magenta-green tracks in HeLa-shPrimPol cells with or without Dox. Error bars, s.d. (**e**) Distribution of IOD values in HeLa-shPrimPol cells with or without Dox (left) or in MEFs derived from WT and *Primpol*$^{-/-}$ mice (right). Horizontal lines in **b**,**c**,**e** represent median values. NS, not significant. $^{***}P < 0.001$ (Mann-Whitney test; **b**,**c**,**e**) and $^{**}P < 0.01$ (Student's *t*-test; **d**). Data are representative of three experiments (**a**), pooled from three experiments (**b**–**d**) and pooled from four experiments with HeLa-shPrimPol cells or three experiments with *Primpol*$^{-/-}$ cells (**e**).

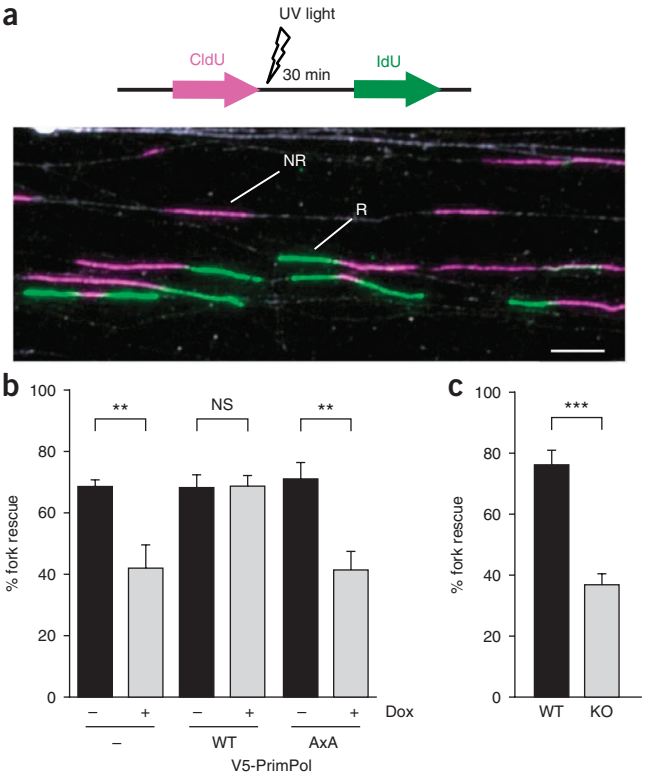

Figure 4 Inefficient restart of stalled forks and activation of dormant origins upon UV irradiation. (**a**) Experimental outline (top) and image of stretched fibers showing magenta-only tracks corresponding to arrested, nonrestarted (NR) forks, and bicolor tracks corresponding to restarted (R) forks (bottom). Scale bar, 10 μm. (**b**) Percentage of fork restart (R/(R + NR)) upon UV irradiation in HeLa-shPrimPol cells with or without Dox treatment. When indicated, plasmids encoding V5-tagged wild-type (WT) or AxA PrimPol versions were transfected. (**c**) Percentage of fork rescue upon UV irradiation in MEFs derived from WT and *Primpol*$^{-/-}$ (KO) mice. Data are representative of three experiments (**a**) and pooled from three experiments (**b**,**c**). Error bars, s.d. $^{**}P < 0.01$ and $^{***}P < 0.001$ (Student's *t*-test).

progression was challenged by HU, which reduces the availability of dNTPs (**Supplementary Fig. 3b**,**c**). This result is in agreement with the enhanced association of PrimPol with chromatin in response to this inhibitor (**Fig. 1b**). We confirmed the partial failure to restart arrested forks upon UV irradiation or HU treatment with *Primpol*$^{-/-}$ MEFs (**Fig. 4c** and **Supplementary Fig. 3c**). We also confirmed all the effects of PrimPol loss on FR, IOD and fork rescue in human diploid fibroblasts (**Supplementary Fig. 3d**–**g**). These results indicate that PrimPol exerts its function by reestablishing DNA synthesis at forks that have been challenged by UV irradiation or dNTP attrition.

Translesion synthesis across UV light–induced photoproducts

Next, we ascertained the biochemical mechanism used by PrimPol to reestablish DNA synthesis at stalled forks. *In vitro*, PrimPol displays both DNA primase and DNA polymerase activities, the latter capable of dealing with abasic sites and oxidized bases as 8-oxoguanine[19]. Given the possible role of PrimPol in mediating fork progression after UV irradiation, we tested whether PrimPol displayed TLS activity on the two main types of template lesions caused by UV irradiation. Purified PrimPol could synthesize DNA across templates carrying either cyclobutane pyrimidine dimers (CPD) or (6-4) pyrimidine

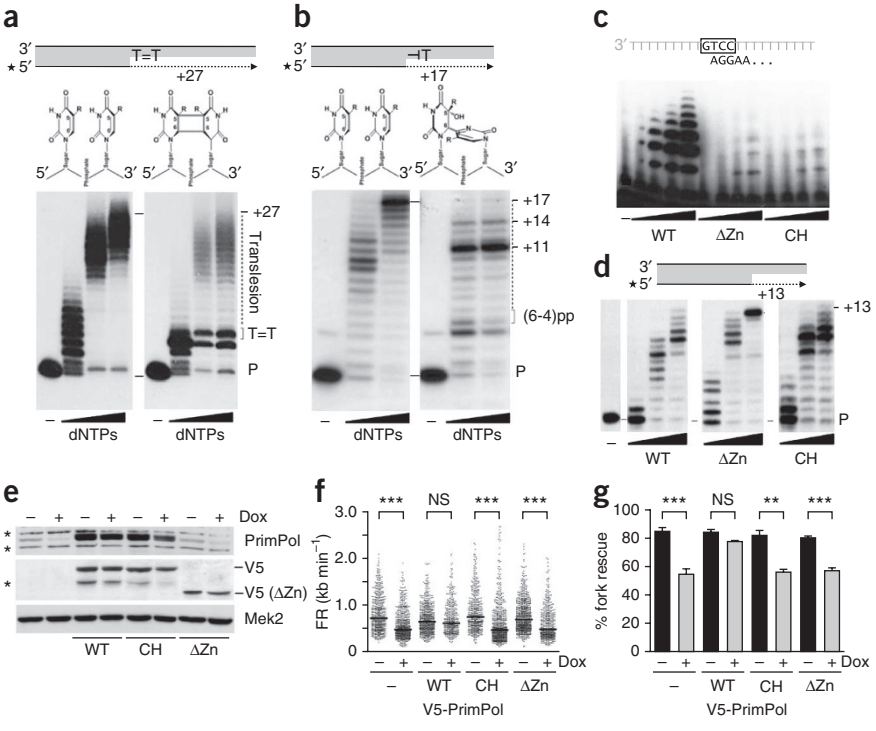

Figure 5 PrimPol TLS synthesis capacity on CPD and (6-4)pp lesions is not sufficient to mediate restart of replication forks. (**a**) Top, schematic of the primer-template structures used for *in vitro* 'running-start' primer-extension assays. Star represents the radioactive label. PrimPol was assayed on a control primer-template structure (left) or a primer template containing a CPD lesion (right). Chemical bonds between the two adjacent thymine bases in the CPD lesion are schematized. Positions of the primer (P) and the CPD adduct (T=T) are indicated in the autoradiogram. dNTPs were omitted (–) or used at 1 μM, 10 μM and 100 μM. (**b**) Similar experimental design as in **a**, but the damaged template contains a (6-4)pp photoproduct. dNTPs were omitted (–) or used at 1 μM and 10 μM. (**c**) *In vitro* primase assay with no protein (–) or increasing concentrations of wild-type (WT), ΔZn or CH versions of PrimPol. Nascent primers initiate at the preferred GTCC sequence (boxed). (**d**) *In vitro* DNA polymerase activity with no protein (–) or increasing concentrations of WT PrimPol and indicated variants in a template-primer molecule with no lesions. (**e**) Immunoblots showing the expression of exogenous PrimPol versions in HeLa-shPrimPol cells, with or without Dox. Asterisks indicate cross-reacting species. The ΔZn deletion mutant migrates faster in SDS-PAGE and can only be detected with anti-V5 antibody. Mek2 is shown as loading control. Uncropped gel images are shown in **Supplementary Figure 7**. (**f**) FR values in HeLa-shPrimPol cells with or without Dox, cotransfected with plasmids expressing WT or mutant PrimPol versions. Horizontal lines represent median values. (**g**) Percentage of fork rescue upon UV irradiation in HeLa-shPrimPol cells with or without Dox, cotransfected with the indicated WT or mutant PrimPol. Error bars, s.d. NS, not significant. $^{**}P < 0.01$ and $^{***}P < 0.001$ (Mann-Whitney test (**f**) and Student's *t*-test (**g**)). Data are representative of five (**a**), four (**b**) and three (**c**–**e**) experiments, and pooled from three (**f**) and four (**g**) experiments.

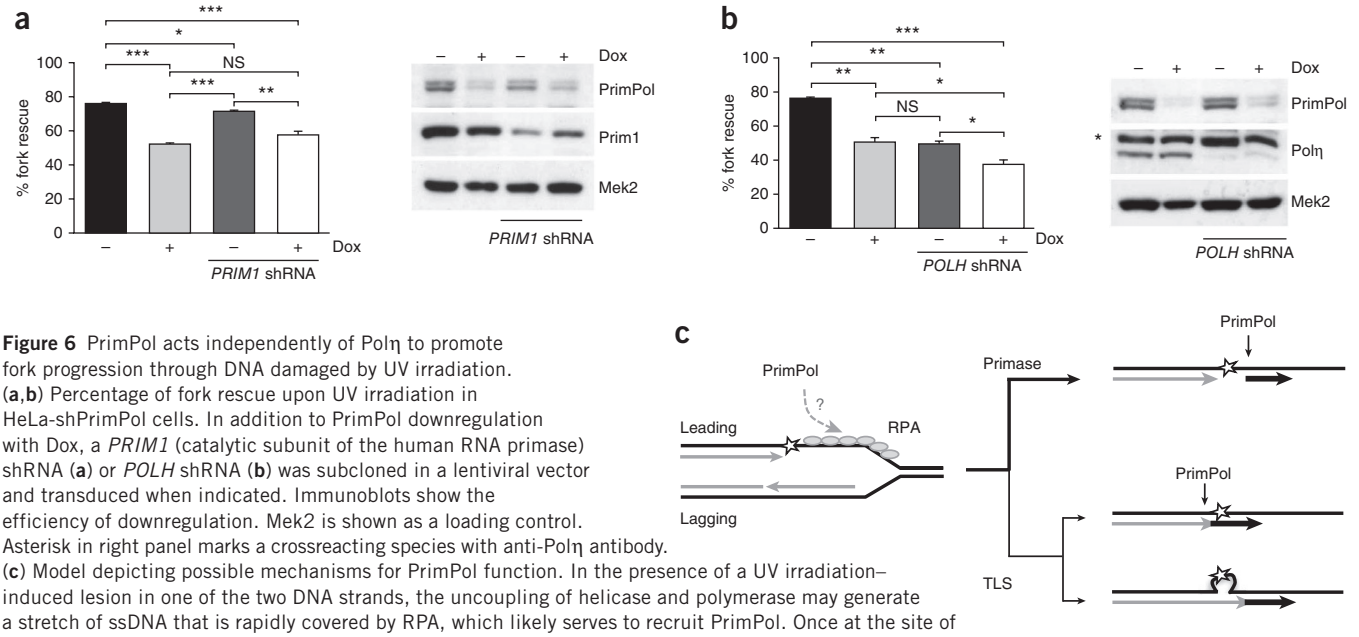

Figure 6 PrimPol acts independently of Polη to promote fork progression through DNA damaged by UV irradiation. (**a**,**b**) Percentage of fork rescue upon UV irradiation in HeLa-shPrimPol cells. In addition to PrimPol downregulation with Dox, a *PRIM1* (catalytic subunit of the human RNA primase) shRNA (**a**) or *POLH* shRNA (**b**) was subcloned in a lentiviral vector and transduced when indicated. Immunoblots show the efficiency of downregulation. Mek2 is shown as a loading control. Asterisk in right panel marks a crossreacting species with anti-Polη antibody. (**c**) Model depicting possible mechanisms for PrimPol function. In the presence of a UV irradiation–induced lesion in one of the two DNA strands, the uncoupling of helicase and polymerase may generate a stretch of ssDNA that is rapidly covered by RPA, which likely serves to recruit PrimPol. Once at the site of damage, PrimPol uses its primase activity to reinitiate a new DNA strand ahead of the lesion, leaving an unreplicated ssDNA gap behind. Alternatively, PrimPol could operate as a TLS polymerase and bypass the lesion directly, although this reaction is inefficient and likely involves a primer-realignment event. Immunoblot data are representative of three experiments (**a**,**b**), data from which were pooled for the histogram analyses. Error bars, s.d. NS, not significant. $*P < 0.05$, $**P < 0.01$ and $***P < 0.001$ (Student's *t*-test).

pyrimidones ((6-4)pp; **Fig. 5a**,**b**). This property is in stark contrast with that of replicative Polε, which was completely blocked by the presence of either lesion (**Supplementary Fig. 4**).

Although PrimPol bypassed the (6-4)pp lesion with high efficiency, the main elongation product was shorter (11 nucleotides added to the primer) than the expected full-length product (+17 nucleotides). The small amount of full-length product suggested that the damaged bases were not copied during primer extension (**Fig. 5b**). We confirmed the accumulation of incomplete products in 'standing-start' assays in which the primer hybridizes just before the damaged nucleotide (**Supplementary Fig. 5a**). In these conditions, bypass of the (6-4)pp adduct strictly depended on the incorporation of dCTP, which is complementary to the template guanine located five positions downstream of the lesion, followed by incorporation of dTTP and dGTP. These results indicate that PrimPol has realigned the primer end to a downstream position, effectively looping out the lesion without copying it (**Supplementary Fig. 5b–e**). This property of PrimPol has also been reported when it bypasses abasic sites[19]. Therefore, in addition to its primase activity, PrimPol has the biochemical potential to bypass CPD or (6-4)pp lesions by performing a 'pseudo-TLS' reaction facilitated by flanking microhomologies.

Restart of stalled forks requires PrimPol primase activity

To evaluate the relative contribution of PrimPol primase and TLS polymerase activities *in vivo*, we took advantage of a truncated version lacking the C-terminal domain that contains the Zn-finger element (**Supplementary Fig. 6a**). In this 'ΔZn' variant, primase activity was largely abolished (**Fig. 5c**), but polymerase activity on normal and damaged templates was preserved (**Fig. 5d** and **Supplementary Fig. 6b**). To control for possible secondary effects of deleting the entire C-terminal domain, we made a double point mutant (CH) in two conserved Zn finger residues; this variant had the same biochemical properties as ΔZn (**Fig. 5c**,**d** and **Supplementary Fig. 6a**,**b**). Thus, both ΔZn and CH turned out to be 'separation of function' mutants in PrimPol. Reintroduction of these primase-dead, polymerase-competent versions into HeLa-shPrimPol cells (**Fig. 5e**) did not rescue any of the phenotypes caused by loss of endogenous PrimPol. We did not observe physiological FRs (**Fig. 5f**), and the frequency of fork recovery upon UV or HU remained lower (**Fig. 5g** and **Supplementary Fig. 6c**). These results indicate that the primase activity of PrimPol is the activity required *in vivo* to resume DNA synthesis at arrested forks, thus implying the synthesis of new primers. By comparison, downregulation of Prim1, the small subunit of Polα–primase complex containing the primase active site, had a modest effect on the ability of stalled forks to continue DNA synthesis (**Fig. 6a**; compare black and dark gray bars). It should be noted, however, that Primase 1 could only be partially downregulated because of its essential function during DNA replication.

PrimPol and TLS Polη have non-overlapping functions

Finally, we compared the efficiency of PrimPol in promoting fork restart *in vivo* with that of bona fide TLS Polη, specialized to synthesize DNA through templates damaged by UV irradiation[24–26]. Polη downregulation impaired fork progression after UV irradiation to a similar extent compared to the loss of PrimPol (**Fig. 6b**, compare dark and light gray bars). The simultaneous downregulation of PrimPol and Polη enhanced the phenotype (**Fig. 6b**, white bar). The effect of the combined knockdown was not as large as the sum of the individual ablation of PrimPol and Polη, but this could be due to the slightly lower levels of downregulation. This result suggests that PrimPol and Polη are not epistatic and perform separate functions during bypass of UV light–induced lesions.

DISCUSSION

The two main mechanisms to replicate damaged DNA in eukaryotic cells are based on translesion synthesis or homologous recombination events. It has been debated whether these reactions take place at the fork, as the replisome is passing through the damaged site, or whether

lesions are initially bypassed and left to be repaired at a later time[9]. These models are not mutually exclusive, but evidence is accumulating in support of the latter. In yeast, postreplicative ssDNA gaps have been visualized by electron microscopy in UV-irradiated cells[11], and genetic experiments have shown that damage tolerance mechanisms can operate uncoupled from DNA replication[27,28]. In chicken DT40 cells, fork progression rates were largely unaffected by disruption of Polη or other TLS components, except for REV1, which provides a noncatalytic function during S phase[29]. In mammalian cells, UV irradiation did not cause persistent fork stalling in cells defective in Polη, but an assay in denaturing conditions revealed the existence of ssDNA gaps in replicated DNA that could collapse into double-strand breaks if not rapidly filled[14].

The lesion-skipping mechanism requires a primase activity to reinitiate DNA synthesis ahead of the damaged site. It could be argued that such a role could be performed by the same primase operating at the origins and Okazaki fragments (for example, dnaG in *Escherichia coli*, Polα-primase in eukaryotes). However, as recently reported, mammalian cells encode a second primase[19] that is functionally related to Archaeal primases but also to bifunctional enzymes having both primase and polymerase activities, a phylogenetically more distant clade belonging to the AEP superfamily[18]. Likely, these enzymes are primitive ancestors of the DNA replication machinery in which two, or even the three basic biochemical activities required at a replication fork (helicase, primase and polymerase) were combined in a single polypeptide. The first protein of this family to be described, encoded by plasmid pRN1 of the archaea *Sulfolobus islandicus*, has an N-terminal region that contains primase and polymerase activities and a C-terminal region that contains a DNA helicase[30]. A similar multifunctional arrangement has been found in poxvirus D5 protein[31] and in *Bacillus cereus* BcMCM, encoded by a prophage integrated in the bacterial genome[32,33]. Human PrimPol also displays primase and polymerase activities but is not a helicase. In all these cases, the primase activity preferentially uses dNTPs, instead of the NTPs required for conventional RNA primases. This specificity of PrimPol enzymes as 'DNA primases' is well-suited for a function in repriming DNA synthesis during continuous elongation (for example, leading-strand synthesis, rolling-circle replication and mitochondrial DNA replication) as it minimizes the need for RNA processing[19].

As shown in this study, PrimPol associates with nuclear chromatin during G1 and S phase, and the rate of fork progression is reduced by its downregulation, even in the absence of exogenous stress. Therefore, we propose that PrimPol has a role during normal DNA replication, probably monitoring fork progression through slow replication zones or other natural challenges. In favor of this notion, PrimPol is needed to rescue forks stalled by HU, which causes temporary dNTP attrition. Our study also showed that PrimPol is rapidly recruited to sites of DNA damage induced by UV irradiation, independently of the checkpoint response. The precise mechanism of PrimPol recruitment remains to be understood, but it could be mediated directly or indirectly by the ssDNA stretches generated by the temporal uncoupling of the DNA helicase and polymerase when the fork hits a damaged site. It is worth mentioning that a mass spectrometry–based search for PrimPol-interacting factors has identified the three components of ssDNA-binding protein RPA after PrimPol immunoprecipitation (S. Mourón, K. Jodkowska, J. Muñoz and J. Méndez; unpublished data).

Once recruited to the site of damage, PrimPol provides arrested forks with two potential mechanisms to move forward: the synthesis of a new primer to reinitiate DNA synthesis downstream of the damage or direct bypass over the lesion using a TLS-like activity (**Fig. 6c**). Our data strongly support the first mechanism, based on the following considerations. First, primase-null PrimPol versions with intact TLS polymerase activity failed to rescue the deficiency in fork progression caused by loss of endogenous PrimPol (**Fig. 4** and **5**, and **Supplementary Fig. 6c**). Second, the TLS activity on templates containing CPD and (6-4)pp lesions was largely incomplete, with the damaged nucleotides probably being looped out rather than copied (**Fig. 5** and **Supplementary Fig. 5**). Third, the fact that PrimPol and Polη, known to efficiently bypass CPD lesions[24,25] have nonredundant functions during rescue of stalled forks *in vivo* (**Fig. 6**). Acording to our data, most UV irradiation–derived lesions will be initially bypassed during DNA replication by repriming events carried out by PrimPol and repaired post-replicatively by Polη, or possibly by homologous recombination if a double-strand break has been generated.

The identification of PrimPol as a new enzyme whose primase activity promotes lesion bypass during nuclear DNA replication opens several questions for the immediate future. Solving the three-dimensional structure of human PrimPol will allow a comparison of its active site with those of PrimPol domain of *Sulfolobus islandicus* pRN1 (ref. 30) and the catalytic subunit (Prim1) of the human RNA primase[34], with the goal of understanding the underlying structural features behind its biochemical properties. It will also be very interesting to define the long-term consequences of PrimPol ablation for a mammalian organism and to search for specific PrimPol mutations in human diseases, such as those recently reported in association with high myopia[35]. Finally, if PrimPol was generally involved in other types of DNA-damage tolerance, its inactivation might increase the efficiency of genotoxic drugs used in chemotherapy.

METHODS

Methods and any associated references are available in the online version of the paper.

Note: Any Supplementary Information and Source Data files are available in the online version of the paper.

ACKNOWLEDGMENTS

We thank all members of our laboratories for helpful discussions, S. Iwai (Osaka University) for the (6-4)pp oligonucleotide, Z.F. Pursell (Tulane University School of Medicine) for purified Polε, J.-S. Hoffmann (Cancer Research Center of Toulouse, France) for anti-Polη, M. Soengas (Spanish National Cancer Research Centre) for HDF cells, P. Delgado for assistance with lymphocyte isolation, M. Pérez and D. Megías for assistance with confocal microscopy and life cell imaging, M.F. Rodríguez-Tornos for her contribution to the early stages of this project, B. Urcelay for technical support in J.M.'s lab, and M. Serrano and A.R. Ramiro for helpful comments on the manuscript. This work was supported by Comunidad de Madrid (S2011/BMD-2361 to L.B.) and the Spanish Ministry of Economy and Competitiveness (BFU2010-21467 to J.M., BFU2012-37969 to L.B., Consolider CSD2007-00015 to L.B. and J.M.).

AUTHOR CONTRIBUTIONS

S.M. and S.R.-A. performed experiments in the cellular system, including single-molecule analysis of DNA replication in stretched fibers. M.I.M.-J. and S.G.-G. performed *in vitro* assays relative to PrimPol biochemical activities. S.C. isolated *Primpol*$^{-/-}$ MEFs. L.B. and J.M. designed the study and led data analysis and interpretation, with contributions from all other authors. J.M. wrote the manuscript.

COMPETING FINANCIAL INTERESTS

The authors declare no competing financial interests.

1. Kelly, T.J. & Stillman, B. in *DNA Replication and Human Disease* (ed. DePamphilis, M.L.) 1–29 (Cold Spring Harbor Laboratory Press, 2006).

2. Lopez-Contreras, A.J. *et al.* A proteomic characterization of factors enriched at nascent DNA molecules. *Cell Rep.* **3**, 1105–1116 (2013).
3. Sirbu, B.M. *et al.* Identification of proteins at active, stalled, and collapsed replication forks using Isolation of proteins on nascent DNA (iPOND) coupled with mass spectrometry. *J. Biol. Chem.* doi:10.1074/jbc.M113.511337 (18 September 2013).
4. Yao, N.Y. & O'Donnell, M. SnapShot: the replisome. *Cell* **141**, 1088 (2010).
5. Conti, C. *et al.* Replication fork velocities at adjacent replication origins are coordinately modified during DNA replication in human cells. *Mol. Biol. Cell* **18**, 3059–3067 (2007).
6. Branzei, D. & Foiani, M. Maintaining genome stability at the replication fork. *Nat. Rev. Mol. Cell Biol.* **11**, 208–219 (2010).
7. Petermann, E. & Helleday, T. Pathways of mammalian replication fork restart. *Nat. Rev. Mol. Cell Biol.* **11**, 683–687 (2010).
8. Tourriere, H. & Pasero, P. Maintenance of fork integrity at damaged DNA and natural pause sites. *DNA Repair (Amst.)* **6**, 900–913 (2007).
9. Sale, J.E., Lehmann, A.R. & Woodgate, R. Y-family DNA polymerases and their role in tolerance of cellular DNA damage. *Nat. Rev. Mol. Cell Biol.* **13**, 141–152 (2012).
10. Zahn, K.E., Wallace, S.S. & Doublie, S. DNA polymerases provide a canon of strategies for translesion synthesis past oxidatively generated lesions. *Curr. Opin. Struct. Biol.* **21**, 358–369 (2011).
11. Lopes, M., Foiani, M. & Sogo, J.M. Multiple mechanisms control chromosome integrity after replication fork uncoupling and restart at irreparable UV lesions. *Mol. Cell* **21**, 15–27 (2006).
12. Callegari, A.J. & Kelly, T.J. UV irradiation induces a postreplication DNA damage checkpoint. *Proc. Natl. Acad. Sci. USA* **103**, 15877–15882 (2006).
13. Callegari, A.J., Clark, E., Pneuman, A. & Kelly, T.J. Postreplication gaps at UV lesions are signals for checkpoint activation. *Proc. Natl. Acad. Sci. USA* **107**, 8219–8224 (2010).
14. Elvers, I., Johansson, F., Groth, P., Erixon, K. & Helleday, T. UV stalled replication forks restart by re-priming in human fibroblasts. *Nucleic Acids Res.* **39**, 7049–7057 (2011).
15. Heller, R.C. & Marians, K.J. Replication fork reactivation downstream of a blocked nascent leading strand. *Nature* **439**, 557–562 (2006).
16. Heller, R.C. & Marians, K.J. Replisome assembly and the direct restart of stalled replication forks. *Nat. Rev. Mol. Cell Biol.* **7**, 932–943 (2006).
17. Langston, L.D. & O'Donnell, M. DNA replication: keep moving and don't mind the gap. *Mol. Cell* **23**, 155–160 (2006).
18. Iyer, L.M., Koonin, E.V., Leipe, D.D. & Aravind, L. Origin and evolution of the archaeo-eukaryotic primase superfamily and related palm-domain proteins: structural insights and new members. *Nucleic Acids Res.* **33**, 3875–3896 (2005).
19. Garcia-Gomez, S. *et al.* PrimPol, an archaic primase/polymerase operating in human cells. *Mol. Cell* doi:10.1016/j.molcel.2013.09.025 (24 October 2013).
20. Jackson, D.A. & Pombo, A. Replicon clusters are stable units of chromosome structure: evidence that nuclear organization contributes to the efficient activation and propagation of S phase in human cells. *J. Cell Biol.* **140**, 1285–1295 (1998).
21. Ge, X.Q., Jackson, D.A. & Blow, J.J. Dormant origins licensed by excess Mcm2–7 are required for human cells to survive replicative stress. *Genes Dev.* **21**, 3331–3341 (2007).
22. Ibarra, A., Schwob, E. & Mendez, J. Excess MCM proteins protect human cells from replicative stress by licensing backup origins of replication. *Proc. Natl. Acad. Sci. USA* **105**, 8956–8961 (2008).
23. Woodward, A.M. *et al.* Excess Mcm2–7 license dormant origins of replication that can be used under conditions of replicative stress. *J. Cell Biol.* **173**, 673–683 (2006).
24. Biertumpfel, C. *et al.* Structure and mechanism of human DNA polymerase eta. *Nature* **465**, 1044–1048 (2010).
25. Johnson, R.E., Prakash, S. & Prakash, L. Efficient bypass of a thymine-thymine dimer by yeast DNA polymerase, Poleta. *Science* **283**, 1001–1004 (1999).
26. Temviriyanukul, P. *et al.* Temporally distinct translesion synthesis pathways for ultraviolet light-induced photoproducts in the mammalian genome. *DNA Repair (Amst.)* **11**, 550–558 (2012).
27. Daigaku, Y., Davies, A.A. & Ulrich, H.D. Ubiquitin-dependent DNA damage bypass is separable from genome replication. *Nature* **465**, 951–955 (2010).
28. Karras, G.I. & Jentsch, S. The RAD6 DNA damage tolerance pathway operates uncoupled from the replication fork and is functional beyond S phase. *Cell* **141**, 255–267 (2010).
29. Edmunds, C.E., Simpson, L.J. & Sale, J.E. PCNA ubiquitination and REV1 define temporally distinct mechanisms for controlling translesion synthesis in the avian cell line DT40. *Mol. Cell* **30**, 519–529 (2008).
30. Lipps, G., Weinzierl, A.O., von Scheven, G., Buchen, C. & Cramer, P. Structure of a bifunctional DNA primase-polymerase. *Nat. Struct. Mol. Biol.* **11**, 157–162 (2004).
31. De Silva, F.S., Lewis, W., Berglund, P., Koonin, E.V. & Moss, B. Poxvirus DNA primase. *Proc. Natl. Acad. Sci. USA* **104**, 18724–18729 (2007).
32. McGeoch, A.T. & Bell, S.D. Eukaryotic/archaeal primase and MCM proteins encoded in a bacteriophage genome. *Cell* **120**, 167–168 (2005).
33. Sanchez-Berrondo, J. *et al.* Molecular architecture of a multifunctional MCM complex. *Nucleic Acids Res.* **40**, 1366–1380 (2012).
34. Kilkenny, M.L., Longo, M.A., Perera, R.L. & Pellegrini, L. Structures of human primase reveal design of nucleotide elongation site and mode of Pol alpha tethering. *Proc. Natl. Acad. Sci. USA* **110**, 15961–15966 (2013).
35. Zhao, F. *et al.* Exome sequencing reveals CCDC111 mutation associated with high myopia. *Hum. Genet.* **132**, 913–921 (2013).

ONLINE METHODS

Antibodies. Anti-PrimPol antibodies (used at an experimental dilution 1:500) were generated in NZW rabbits immunized with a KLH-conjugated peptide corresponding to the 14 C-terminal amino acids of human PrimPol and affinity-purified against the peptide used as antigen[19] (Thermo Fisher Scientific). Anti-Mcm2 (1:2,000) has been described[36]. The following commercial antibodies were used: 53BP1 (Novus Biologicas NB-100-304; 1:500), BrdU (FITC-conjugated, BD Pharmingen 556028; 1:50), CldU (rat monoclonal anti-BrdU, Abcam ab6326; 1:100), CTCF (Millipore 07-729; 1:1,000), γH2AX (Millipore 05-636; 1:200), IdU (mouse monoclonal anti-BrdU, BD 347580; 1:100), Mek2 (BD Biosciences Pharmingen 610236; 1:2,000), PCNA (Santa Cruz SC-56; 1:1,000), Polη (Abcam ab17725; 1:1,000), Prim1 (p48 Primase, Cell Signaling 8G10; 1:1,000), RPA32 (Cell Signaling 2208S; 1:200), ssDNA (Millipore MAB3034; 1:100), α-tubulin (Sigma T9026; 1:500), γ-tubulin (Sigma T5326; 1:1,000) and V5 (Invitrogen 46-0705; 1:1,000). Secondary antibodies used for immunofluorescence were from Invitrogen Molecular Probes and used at a 1:200 dilution: anti-rabbit IgG AF-488 (chicken), anti-mouse IgG AF-488 (goat) and AF-647 (donkey), anti-rat IgG AF-488 (chicken) and AF-594 (goat), anti-mouse IgG2a AF-647 (goat). Horseradish peroxidase–linked ECL anti-rabbit IgG (GE Healthcare NA934V) and anti-mouse IgG (GE Healthcare; NA931V) were used at 1:5,000. For all commercial antibodies, validation and specificity examples are provided in the manufacturer's instructions.

Cell lines and manipulations. HeLa and U2OS were obtained from the Spanish National Cancer Research Center repository. HDF (human diploid fibroblasts) were provided by M. Soengas (Spanish National Cancer Research Center) and MEFs (mouse embryonic fibroblasts) were specifically generated for this study. All cells were grown in DMEM supplemented with 10% FBS plus penicillin-streptomycin. Cell lines were tested monthly for mycoplasma contamination. T lymphocytes were isolated from mouse spleen using CD43 (Ly-48) magnetic microbeads (Miltenyi Biotec) and cultured in RPMI supplemented with 10% FBS, 10 mM HEPES, 50 μM β-mercaptoethanol and 3 μg/ml Concanavalin A (Sigma) to stimulate proliferation.

Stable cell lines HeLa-shPrimPol, U2OS-shPrimPol and HDF-shPrimPol were generated by infection of a TRIPZ lentiviral vector carrying an inducible shRNAmir targeting the sequence 5′ TGCTGTTGACAGTGAGCG in the 3′ untranslated region (UTR) of *PRIMPOL* gene (Open Biosystems). Expression of *PRIMPOL* shRNAmir was induced with 1 μg/ml doxycyclin (Dox) for 3 d. For *PRIM1* and *POLH* downregulation, GIPZ lentiviral shRNAmir vectors targeting the sequence 5′ ATATCTTGATTAACCAAGG in the 3′ UTR of *Prim1* and 5′ TGCTTTAGAGGATTCTTCT in the 3′ UTR of the gene encoding Polη were used (Open Biosystems). DNA sequences encoding wild-type (WT) PrimPol, AxA, a Zn-finger mutant (CH) and ΔZn were cloned into Gateway expression vectors introducing an N-terminal V5 or GFP tag (Invitrogen). Transient transfections were performed using Lipofectamine 2000 (Invitrogen).

For cell proliferation assays, aliquots of 0.8×10^5 cells were seeded in complete medium and counted every 2 d in a hemocytometer. When indicated, cells were treated with either 10 μM aphidicolin (Sigma) or 2 mM hydroxyurea (Sigma) for 2 h, or irradiated with UVC (30 J/m^2) or γ-IR (10 Gy) half an hour or an hour, respectively, before harvesting. To inhibit the ATR-Chk1 checkpoint response, 7.5 mM caffeine (Sigma) or 0.4 μM UCN-01 (Sigma) were added to the medium 1 h before the addition of HU. To achieve culture synchronization, cells were incubated with 2.5 mM thymidine (Sigma) for 20 h and released in fresh medium for 0 h (G1-S phase), 5 h (S phase), 9 h (G2-M phase) and 14 h (following G1 phase). For DNA-content analysis, cells were fixed in 70% ethanol, washed in PBS and stained with 50 μg/ml propidium iodide (Sigma) in the presence of 10 μg/ml RNase A (Qiagen). For the cytometry detection of BrdU incorporation, 10 μM BrdU (Sigma) was added to the medium for 30 min before cell harvesting. Fixed cells were treated with 2 M HCl for 20 min, and BrdU was immunolabeled with FITC-conjugated anti-BrdU. Flow cytometry data were acquired in a FACSCanto cytometer (BD Biosciences) and analyzed with FlowJo software (Tree Star Inc.).

Quantitative PCR. Total RNA was extracted with Trizol (Invitrogen), treated with DNAse I and subjected to standard purification with phenol: chloroform. 4 μg of total RNA were used for random-priming cDNA synthesis with SuperScript II (Invitrogen). Quantitative PCR was performed with Power SYBR Green master mix (Applied Biosystems) according to manufacturer's instructions.

Extract preparation, biochemical fractionation and immunoblots. Whole-cell extracts were prepared by direct suspension of cells in Laemmli buffer followed by three pulses of sonication for 15 s at 15% amplitude (Branson Digital Sonifier). Biochemical fractionation was performed as described[37]. SDS-PAGE, protein transfer to nitrocellulose membranes and immunoblots were performed using standard protocols[38]. Immunoblot signals were quantified using ImageJ software[39].

Immunofluorescence microscopy. Cells grown on glass coverslips were fixed in 4% paraformaldehyde (PFA) for 10 min and permeabilized with 0.5% Triton X-100 (10 min at room temperature (RT)). Coverslips were incubated in blocking solution (3% bovine serum albumin (BSA) in PBS) for 30 min. Primary antibody solution was applied for 1 h at RT. For RPA, PCNA and 53BP1 immunostaining, soluble proteins were preextracted before fixation in CSK buffer (10 mM Pipes-KOH pH 7.0, 100 mM NaCl, 300 mM sucrose and 3 mM $MgCl_2$) supplemented with 0.5% Triton X-100. Cell nuclei were stained with DAPI (Sigma). Coverslips were mounted onto glass microscope slides using Mowiol (Calbiochem). Images were acquired in a Leica-TCS SP5X confocal microscope, with a HCX PL APO 63× 1.4 numerical aperture (NA) oil-immersion objective using LAS AF version 2.5.1 software. To estimate RPA foci-positive cells, 800–1,000 HeLa-shPrimPol nuclei (300–500 MEFs) were scored in each condition. To estimate the abundance of misaligned or lagging chromosomes, 100–200 cells at metaphase and 50 cells at anaphase were scored in each assay. For micronuclei, 1,000 cells at interphase were scored in each assay.

High-throughput microscopy analysis. HeLa cells were grown on μCLEAR bottom 96-well plates (Greiner Bio-One) and γH2AX immunofluorescence was performed using standard procedures[38]. Images were automatically acquired from each well by an Opera High-Content Screening System (PerkinElmer) with an APO 20×, 0.7 NA water-immersion objective. Images were analyzed with Acapella software (PerkinElmer). Nuclei were segmented using the DAPI staining, and then γH2AX intensity was measured within the nuclei mask.

Live cell imaging. HeLa and U2OS cells expressing GFP-tagged PrimPol were grown on chambered coverslips (Ibidi) at 37 °C and 5% CO_2. Cells with intermediate fluorescence level were selected to be locally microirradiated with a 405-nm diodide laser. Hoeschst 33342 (Invitrogen) was added to the medium at 20 ng/ml before irradiation. Nuclear damage was induced with two pulses of laser at 60% AOTF. Images were taken every 1 min during 60 min using a Leica-TCS SP5X confocal microscope, with a HCX PL APO 63×, 1.3 NA glycerol-immersion objective using LAS AF version 2.5.1 software. Live cell imaging was carried out in parallel with cells expressing GFP-tagged 53BP1 and H2Ab, as positive and negative controls of response to laser, respectively.

Preparation of mitotic spreads. T-lymphocyte culture medium was supplemented with 0.4 μM aphidicolin for 24 h and then with 0.1 μg/ml colcemid (Gibco) for 2 h. Cells were incubated in a hypotonic solution (75 mM KCl) for 20 min at 37 °C, fixed with 3:1 methanol:acetic acid, dropped onto microscope slides and stained with 5% Giemsa (Sigma). Images were recorded with an Olympus BX microscope and CytoVision 3.1 software (Applied Imaging Corporation). In each assay, 80 metaphase cells were scored for chromosome breaks, gaps or fusions.

Single-molecule analysis of DNA replication in stretched fibers. Cells growing exponentially in culture were pulse-labeled with 50 μM CldU (20 min) followed by 250 μM IdU (20 min). Labeled cells were harvested and resuspended in 0.2 M Tris pH 7.4, 50 mM EDTA and 0.5% SDS. Stretched DNA fibers were prepared as described[40] with minor modifications. A detailed protocol is available on request. To evaluate fork restart, cells were first pulsed with CldU for 20 min and then irradiated with UVC (30 J/m^2) or treated with 5 mM HU (Sigma) for 5 h. 30 min after exposure to UV light, or immediately after the HU incubation, cells were pulsed with IdU for 20 min in fresh medium. For immunodetection of labeled tracks, fibers were incubated with primary antibodies for 1 h at RT and the corresponding secondary antibodies for 30 min at RT, in a humidity chamber.

doi:10.1038/nsmb.2719

CldU tracks, originally red, have been recolored in magenta to facilitate contrast detection by readers with colorblindness. DNA was stained with anti-ssDNA to assess fiber integrity. Fiber images were obtained in a DM6000 B Leica microscope with an HCX PL APO 40×, 0.75 NA objective. The conversion factor used was 1 μm = 2.59 kb[20]. In each assay, >300 tracks were measured for FR estimation, >50 fibers containing two or more origins were analyzed for IOD and >500 tracks were measured to estimate percentage of fork restart.

Expression and purification of PrimPol versions with an altered Zn finger. The deletion mutant ΔZn was constructed by PCR amplification of the first 1227 nucleotides of the human *CCDC111* cDNA (cloned in plasmid pET16::CCDC111; ref. 19), flanked by NdeI and BamHI sites. The amplified product was inserted in the *Escherichia coli* expression plasmid pET16 (Novagen). The double point mutant CH, designed to change Cys419 to glycine and His426 to tyrosine, was generated with the QuikChange Site-Directed Mutagenesis kit (Stratagene). All *CCDC111* mutants were confirmed by sequencing. Recombinant PrimPol variants (ΔZn and CH) were overexpressed in *E. coli* and purified as described[19].

DNA primase assay. DNA primase activity of the ΔZn and CH mutants was evaluated using a 29-mer oligonucleotide (5′-T_{15}CCTGT_{10}-3′) as template, which contains a putative herpes virus priming initiation site (GTCC), as described[19]. The reaction mixture (20 μl) contained buffer R (50 mM Tris pH 7.5, 5% Gly, 75 mM NaCl, 1 mM $MnCl_2$, 1 mM DTT and 0.1 μg/μl BSA), [γ-^{32}P]ATP (16 nM; 3,000 Ci/mmol), 10 μM dGTP and various concentrations of either wild-type PrimPol, or ΔZn or CH variants (50, 100, 200 and 400 nM). The reaction was incubated during 60 min at 30 °C. Reactions were stopped by addition of formamide loading buffer (10 mM EDTA, 95% v/v formamide and 0.3% w/v xylene-cyanol) and loaded in 8 M urea–containing 20% polyacrylamide sequencing gels.

DNA polymerase activity. A 15-mer oligonucleotide primer (5′-GATC ACAGTGAGTAC-3′) was labeled using T4 PNK (New England BioLabs) and [γ-^{32}P]ATP (3,000 Ci/mmol), and hybridized to a 28-mer oligonucleotide template (5′-AGAAGTGTATCTCGTAC TCACTGTGATC-3′) in 20 mM Tris, 0.5 M NaCl, heated up to 80 °C and cooled down to RT. The resulting hybrid had a 5′ protrusion of 13 templating nucleotides. The reaction mixture (20 μl) in buffer R contained 5 nM [γ-^{32}P]-labeled template-primer, 100 μM dNTP and either wild-type PrimPol, or ΔZn or CH mutants (50, 100 and 200 nM). The reaction was incubated during 60 min at 30 °C. Reactions were stopped and analyzed as in the DNA primase assay.

TLS activity. A 5′-^{32}P–labeled primer (5′-CCGTACGATCATACTGAC-3′) was hybridized to a template containing a cyclobutane pyrimidine dimer (CPD; T-T) embedded in the sequence 5′-AGGATAGTGACAGTAGTGTATG(T-T) ATAGTCAGTATGATCGTACGG-3′ as described above. This CPD-containing substrate has a 3′ protrusion of 27 template nucleotides. A 5′ ^{32}P labeled primer (5′-CACTGACTGTATG-3′) was hybridized to a template containing a (6-4)pp photoproduct (5′-CTCGTCAGCATC(6-4)CATCATACAGTCAGTG-3′), kindly provided by S. Iwai (Osaka University). This (6-4)pp-containing substrate structure has a 3′ protrusion of 17 template nucleotides. The reaction mixture (20 μl) in buffer R contained 5 nM [γ-^{32}P]-labeled template-primer containing one of the lesions indicated above, 200 nM of either wild-type PrimPol, or ΔZn or CH mutants, and increasing amounts of dNTPs. The reaction was incubated during 60 min at 30 °C. When indicated, human PrimPol was substituted by human Polε (2 nM), provided by Z.F. Pursell (Tulane University School of Medicine). In this case, TLS of CPD and (6-4)pp was evaluated in 50 mM Tris pH 7.5, 5% glycerol, 1 mM DTT, 0.1 μg/μl BSA, 50 mM NaCl and 8 mM $MgCl_2$ at different dNTP concentrations, and reactions were incubated for 30 min at 37 °C. Polymerization products were analyzed in 8 M urea–containing 20% polyacrylamide sequencing gels.

Statistical methods. In column graphs, data are expressed as mean ± s.d. Statistical analyses were done with two-tailed Student's *t*-test. When the data are presented in scatter dot plots, the bar corresponds to the median value. For the analyses of FR or IOD parameters in stretched DNA fibers, the data distribution is normally not Gaussian, and differences between samples were assessed with the nonparametric Mann-Whitney rank-sum test[41]. Statistical analysis was performed in Prism v4.0 (GraphPad Software).

36. Ekholm-Reed, S. *et al.* Deregulation of cyclin E in human cells interferes with prereplication complex assembly. *J. Cell Biol.* **165**, 789–800 (2004).
37. Mendez, J. & Stillman, B. Chromatin association of human origin recognition complex, cdc6, and minichromosome maintenance proteins during the cell cycle: assembly of prereplication complexes in late mitosis. *Mol. Cell. Biol.* **20**, 8602–8612 (2000).
38. Harlow, E. & Lane, D. in *Using Antibodies: a Laboratory Manual* (Cold Spring Harbor Laboratory Press, 1998).
39. Schneider, C.A., Rasband, W.S. & Eliceiri, K.W. NIH Image to ImageJ: 25 years of image analysis. *Nat. Methods* **9**, 671–675 (2012).
40. Terret, M.E., Sherwood, R., Rahman, S., Qin, J. & Jallepalli, P.V. Cohesin acetylation speeds the replication fork. *Nature* **462**, 231–234 (2009).
41. Bianco, J.N. *et al.* Analysis of DNA replication profiles in budding yeast and mammalian cells using DNA combing. *Methods* **57**, 149–157 (2012).